L-type voltage-gated Ca^{2+} channel $Ca_V1.2$ regulates chondrogenesis during limb development

Yuji Atsuta[a,b], Reiko R. Tomizawa[a,b], Michael Levin[b,c], and Clifford J. Tabin[a,b,1]

[a]Department of Genetics, Harvard Medical School, Boston, MA 02115; [b]Allen Discovery Center at Tufts University, Tufts University, Medford, MA 02155; and [c]Department of Biology, Tufts University, Medford, MA 02155

Contributed by Clifford J. Tabin, September 3, 2019 (sent for review May 24, 2019; reviewed by Cheng-Ming Chuong and Min Zhao)

All cells, including nonexcitable cells, maintain a discrete transmembrane potential (V_{mem}), and have the capacity to modulate V_{mem} and respond to their own and neighbors' changes in V_{mem}. Spatiotemporal variations have been described in developing embryonic tissues and in some cases have been implicated in influencing developmental processes. Yet, how such changes in V_{mem} are converted into intracellular inputs that in turn regulate developmental gene expression and coordinate patterned tissue formation, has remained elusive. Here we document that the V_{mem} of limb mesenchyme switches from a hyperpolarized to depolarized state during early chondrocyte differentiation. This change in V_{mem} increases intracellular Ca^{2+} signaling through Ca^{2+} influx, via $Ca_V1.2$, 1 of L-type voltage-gated Ca^{2+} channels (VGCCs). We find that $Ca_V1.2$ activity is essential for chondrogenesis in the developing limbs. Pharmacological inhibition by an L-type VGCC specific blocker, or limb-specific deletion of $Ca_V1.2$, down-regulates expression of genes essential for chondrocyte differentiation, including *Sox9*, *Col2a1*, and *Agc1*, and thus disturbs proper cartilage formation. The Ca^{2+}-dependent transcription factor NFATc1, which is a known major transducer of intracellular Ca^{2+} signaling, partly rescues Sox9 expression. These data reveal instructive roles of $Ca_V1.2$ in limb development, and more generally expand our understanding of how modulation of membrane potential is used as a mechanism of developmental regulation.

limb development | chondrogenesis | membrane potential | calcium channel

Although most often thought of in the context of excitable cells such as neurons, all cells maintain, and respond to changes in, transmembrane potential (the difference in electric voltage between the interior and exterior of a cell, V_{mem}). Changes in V_{mem} are involved in a wide variety of cellular behaviors including cellular proliferation, survival, differentiation and motility (1). These V_{mem} changes are mainly determined by ion influx/efflux, mediated by channels, pumps, and gap-junctions embedded in the plasma membrane (2). As some ion channels are expressed with temporal and tissue specificity, endogenous spatiotemporal gradients of V_{mem} can be generated across tissues and organs (1). Consistent with this, changes in V_{mem} are known to influence embryonic development, among other processes (2–11).

The impacts of changes in V_{mem} (depolarization or hyperpolarization) are often mediated through the opening or closing of voltage-sensitive ion channels, such as the voltage-gated Ca^{2+} channel (VGCC) (12, 13). The extracellular Ca^{2+} concentration is thousands of times higher than the intracellular concentration under physiological conditions, hence the opening of VGCCs by membrane depolarization allows Ca^{2+} ions to flow into cells (14). In addition to mediating action potentials in excitable cells, cytoplasmic Ca^{2+} ions entering through VGCCs act as intracellular second messengers, activating several downstream signaling pathways, such as the calmodulin (CaM)/calcineurin and the PKC/MAPK pathways. The cellular impact of VGCC activation has been particularly well studied in the context of muscle differentiation (15, 16), and neuronal proliferation, migration, and differentiation (17, 18). However, VGCCs are also found in nonexcitable cells (19). For example, $Ca_V2.1$, a P/Q- type VGCC, is abundant on the membrane of human red blood cells (20), and $Ca_V1.2$, L-type, and $Ca_V3.2$ T-type VGCCs are expressed in murine chondrocytes and osteoblasts (21). At a functional level, $Ca_V3.2$ has been shown to play an essential role in tracheal cartilage formation (22). VGCCs are also correlated with congenital malformations in humans, including the presence of syndactyly in Timothy syndrome patients who carry a heterozygous mutation in the *CACNA1C* gene encoding the pore-forming subunit of $Ca_V1.2$ (23). Despite these intriguing findings, however, the elucidation of definitive roles for V_{mem} and voltage-gated Ca^{2+} channels in development, especially in amniotes, has remained elusive.

Here we take advantage of the well-studied developing chick and mouse limb systems to decipher how spatiotemporal changes of V_{mem} and subsequent VGCC's activation regulate organogenesis. We find that the mesenchymal cells of the early limb bud are initially hyperpolarized. Strikingly, however, cells in the core of the limb bud became depolarized during chondrogenic differentiation. This depolarization stimulates Ca^{2+} transients controlled by L-type VGCCs. We show that intracellular Ca^{2+} signals are sufficient to regulate chondrogenesis of cultured limb cells in vitro. Moreover, the voltage-gated calcium channel $Ca_V1.2$ is essential for proper chondrocyte development in the developing limb in vivo, at least in part, mediated by the Ca^{2+} signaling-dependent transcription factor, NFATc1. Taken together, our results establish a critical role for V_{mem} in controlling differentiation and patterning during embryonic development.

Significance

Membrane potential is the difference in electric potential between the inside and outside of a cell. Cells can alter their membrane potential through modulating ion channels and pumps. The role of membrane potential has been well studied in a variety of settings, including as a mechanism of coding and transmitting information in neurons. However, far less is known about the role of regulated membrane potential in other contexts, such as in cell fate decisions during embryonic morphogenesis. We show a critical role for membrane depolarization in triggering chondrogenesis during limb development, mediated through the opening of a voltage-gated Ca^{2+} channel, $Ca_V1.2$, which in turn activates expression of downstream genes, expanding our knowledge of the role bioelectric signals play in development.

Author contributions: Y.A., M.L., and C.J.T. designed research; Y.A. and R.R.T. performed research; M.L. contributed new reagents/analytic tools; Y.A. and R.R.T. analyzed data; and Y.A. and C.J.T. wrote the paper.

Reviewers: C.-M.C., University of Southern California; and M.Z., University of California, Davis.

The authors declare no competing interest.

Data deposition: The raw data for quantifications including Alicia blue staining, quantitative PCR data, cell counting, and length measurements of mouse limbs have been deposited at https://bitbucket.org/tabinlab/pnas-01908981/.

[1]To whom correspondence may be addressed. Email: tabin@genetics.med.harvard.edu.

This article contains supporting information online at www.pnas.org/lookup/suppl/doi:10.1073/pnas.1908981116/-/DCSupplemental.

First published October 7, 2019.

Results

Limb Mesenchyme Is Depolarized during Chondrogenic Differentiation. The developing limb bud is 1 of the most intensely studied and best understood models for vertebrate pattern formation and morphogenesis. To see whether significant changes in V_{mem} take place during limb development, we stained slice cultures of mouse limb buds at embryonic day (E)10.5 (when the early limb bud mesenchyme is morphologically uniform and undifferentiated), E11.5 (when differentiation has started in the proximal limb), and E12.5 (when the distal limb is undergoing differentiation), using the potential sensitive fluorescent dye $DiBAC_4(3)$ (Fig. 1 *A* and *B*). DiBAC is a charged molecule and hence is excluded from hyperpolarized cells, while it is taken up and concentrated in depolarized cells, allowing its use as a fluorescent voltage reporter in vivo (24). DiBAC staining was not observed in limb mesenchyme at E10.5, indicating that early limb bud progenitors have polarized V_{mem}. The polarized state of the early limb mesenchyme was confirmed by staining slice cultures with the low voltage-sensitive dye CC2-DMPE (*SI Appendix*, Fig. S1*A*). Moreover, DiBAC staining of the early limb bud mesenchyme could be induced by treating slice cultures with 40 mM potassium (K)-gluconate solution, which forces their depolarization (25) (*SI Appendix*, Fig. S1*B*). In contrast, at E11.5 and E12.5, areas of DiBAC staining became evident in the core of the limb buds in domains that correlated with regions of chondrogenesis, identified by Col2 staining of parallel slice cultures (Fig. 1*C*). Similar results were obtained with developing chick limb buds of an equivalent stage (*SI Appendix*, Fig. S1*C*).

To verify that the depolarization we observed in later-stage limb buds was associated with chondrogenic differentiation, we turned to "micromass culture," a well-established in vitro system for studying chondrogenesis of limb morphogenesis. When early limb bud cells are dissociated and placed into culture at high density, they spontaneously undergo differentiation, most prominently into chondrocytes (26). Micromass cultures were established from transgenic mice carrying a *Col2a1*-tdTomato reporter that produces a red fluorescent signal in chondrocytes, the cell type that expresses the endogenous *Col2al* gene. Although the micromass cultures are confluent, with no space between cells, focal tdTomato staining becomes evident after 2 d of culture, representing groups of cells undergoing chondrogenesis (Fig. 1 *D* and *E*). DiBAC produces a similar pattern of positively staining puncta, and merged images demonstrate that the DiBAC and tdTomato signals are indeed colocalized.

In principle, the depolarization we observe in the developing limb mesenchyme could play a key role in regulating chondrogenesis, or alternatively, it could be a consequence of chondrogenic differentiation. To differentiate between these possibilities, we turned to the signals potentially upstream of the change we observed in V_{mem}. In many cells where changes in membrane potential are observed, it is the opening of Na^+ channels that is responsible for membrane depolarization. Moreover, at least 2 Na^+ channels are known to be expressed in the limb membrane, $Na_V1.4$ and the epithelial Na^+ channel (ENaC) (27, 28). As tetrodotoxin, a specific inhibitor of Na_V channels, does not have an effect on cartilage formation in micromass-cultured chick cells (28), we focused on the potential role of ENaC. When we treated chick micromass-cultured cells with Benzamil (a selective ENaC blocker), we observed a noted decrease in DiBAC staining after 2 d in culture, indicating that ENaC plays a significant role in the depolarization of chondrogenic cells in the limb (*SI Appendix*, Fig. S2*A*). Moreover, when chondrogenesis was assessed in these cultures via Alcian blue staining (a dye that binds to the acidic proteoglycan-rich cartridge matrix), we saw a dose-dependent decrease in chondrogenic differentiation (*SI Appendix*, Fig. S2 *B* and *C*), indicating that membrane depolarization acts upstream of chondrogenic differentiation in the developing limb bud.

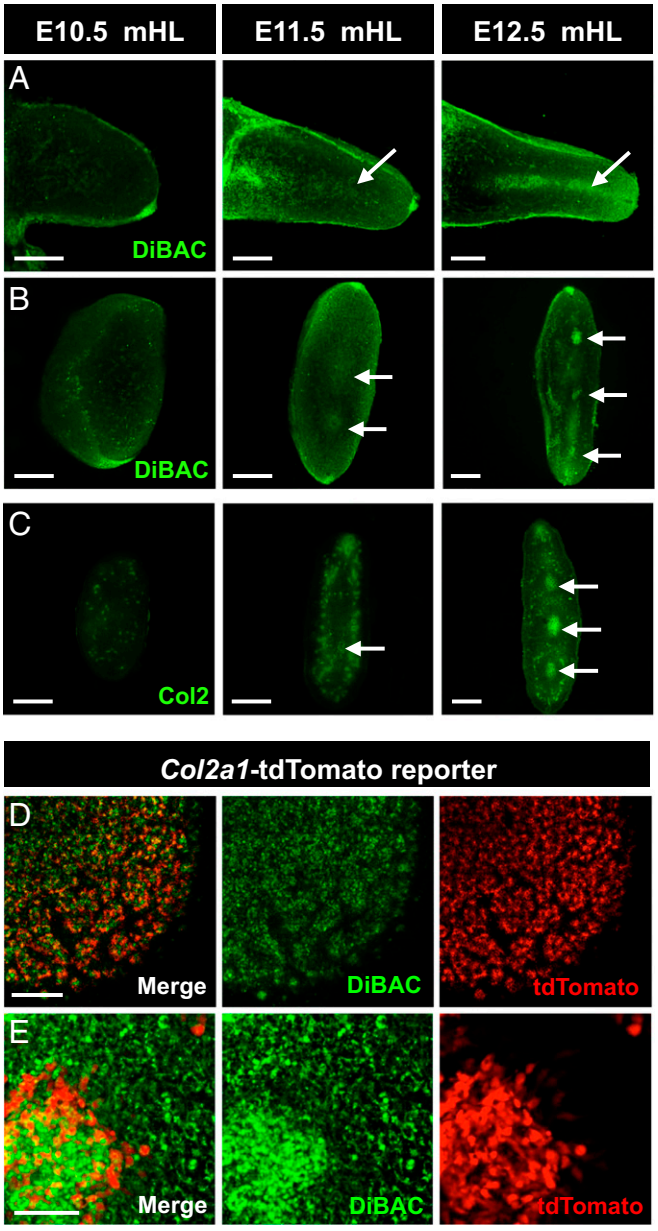

Fig. 1. Depolarization during chondrogenic differentiation of limb mesenchyme cells. (*A* and *B*) Transverse (*A*) and sagittal sections (*B*) of mouse hindlimbs at E10.5, E11.5, and E12.5. $DiBAC_4(3)$ (DiBAC) signals are indicated by arrows. (*C*) Sagittal sections of mouse hindlimbs labeled with immunostaining against Col2a1. (*D* and *E*) Limb mesenchyme from *Col2a1*-tdTomato reporter mice was micromass-cultured in the presence of 4-OHT for 2 d, and stained with DiBAC. (Scale bars: 200 μm in *A*–*C*, 1 mm in *D*, and 100 μm in *E*.)

Depolarization of Limb Mesenchyme Increases Ca^{2+} Transients in L-Type Voltage-Gated Ca^{2+} Channel-Dependent Manner. To determine the mechanism by which the V_{mem} regulates chondrogenesis, we next investigated the immediate consequences of changes in membrane potential in the limb bud mesenchyme. One of the main ways cells respond to membrane potential is through changes in activity of voltage-gated channels, including the VGCCs. Thus, we asked if the depolarization would cause an increase in Ca^{2+} influx in differentiating micromass cultures of limb mesenchyme taking advantage of GCaMP, a genetically encoded Ca^{2+} sensor (29, 30). An RCAS-viral vector transducing GCaMP6s-2A-mCherry was transfected into early chick limb buds, and intracellular Ca^{2+} dynamics was monitored at a single-cell level (Fig. 2 and Movies S1–S6). GCaMP

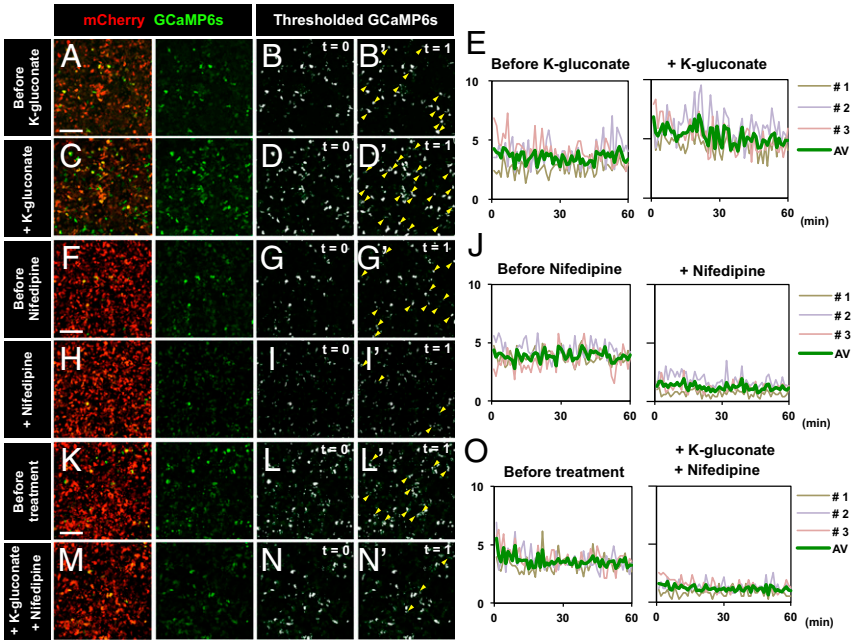

Fig. 2. Ca^{2+} transients in limb mesenchyme are regulated by voltage-gated L-type Ca^{2+} channels. (*A–O*) Live-imaging analyses of Ca^{2+} transients visualized with GCaMP6s in micromass-cultured chicken limb bud cells. mCherry was co-overexpressed as a control signal. The micromass-cultured cells were treated with K-gluconate (40 mM; *C* and *D*), Nifedipine (250 μM; *H* and *I*) or both (*M* and *N*). At each time point, images were thresholded to visualize GCaMP transients and newly emerged GCaMP signals were counted as GCaMP transients, as marked by yellow arrowheads in (*B′*, *D′*, *G′*, *I′*, *L′*, and *N′*). (*E*, *J*, and *O*) Temporal dynamics of GCaMP transients ($n = 3$ each). Time-lapse analyses started 5 h after plating. GCaMP flashes were counted every minute for 60 min. (Scale bars: 100 μm in *A*, *F*, and *K*.)

transients, indicative of Ca^{2+} flux, occurred in 3.6% (average 3.56%) of the transfected ($mCherry^{+}$) cells (Fig. 2 *A*, *B*, and *E*). We then artificially drove depolarization of these cells by treatment with K-gluconate. This resulted in an increase in frequency of the Ca^{2+} transients to 5.27% ($P < 0.01$ vs. control), implying that VGCCs are activated in response to depolarization (Fig. 2 *C–E*).

There are a number of classes of VGCCs mediating the entry of Ca^{2+} ions upon depolarization. Prominent among these are the L-type VGCCs. To test whether L-type VGCCs were responsible for the observed elevation of Ca^{2+} signals in depolarized limb mesenchyme, the GCaMP-expressing cells were cultured with Nifedipine, a drug that specifically blocks the function of L-type VGCCs (Fig. 2 *F–J*). Before Nifedipine administration, about 3.9% of the cells exhibited Ca^{2+} transients (Fig. 2 *F*, *G*, and *J*). In the presence of Nifedipine, Ca^{2+} fluctuation was significantly attenuated, with only 1.23% of the cells displaying transients (Fig. 2 *H–J*) ($P < 0.01$). Moreover, even when depolarization was artificially driven in the cultures by exposure to K-gluconate, Nifedipine prevented the cells from elevating their rate of Ca^{2+} transients (Fig. 2 *K–O*) (3.61% before treatment, 1.2% in treated groups, $P < 0.01$).

Interestingly, the effect of Nifedipine is only observed when cultures are treated during the first day of micromass culture. When similar cultures were compared following treatment with or without Nifedipine 2 d later, we observed no difference in percent of Ca^{2+} transients (*SI Appendix*, Fig. S3) (2.21% before treatment, 2.1% in treated groups, $P = 0.056$) (Movies S7 and S8). At day 2 of micromass cultures, we observed elongated-shaped myoblast-like cells, Ca^{2+} transients of which were completely suppressed by Nifedipine, and we disregarded these cells since the cells were not derived from limb mesenchyme. This unchanged frequency of Ca^{2+} transients in differentiating limb mesenchyme suggests that the role of L-type VGCCs in controlling Ca^{2+} flux is limited to the undifferentiated limb mesenchymal cells, and that they do not play such a role once chondrogenic differentiation has commenced.

L-Type Ca^{2+} Channels Regulate Cartilage Formation In Vitro. Our results indicate that V_{mem} effects both Ca^{2+} flux (via L-type VGCCs) and chondrogenesis in limb mesenchyme. To see whether the induced Ca^{2+} transients are themselves responsible for the regulation of chondrogenesis, micromass-cultured chick limb cells were treated with either Nifedipine to block Ca^{2+} influx through L-type VGCCs, or a Ca^{2+} ionophore, A23187 (also known as calcimycin), to increase the level of Ca^{2+} entering the cells. Nifedipine treatment down-regulated chondrogenesis, as assessed by Alcian blue staining, whereas A23187 increased Alcian blue staining, each in a concentration-dependent manner (Fig. 3 *A* and *B*). To verify this finding, qPCR was performed for markers of early- (*Sox9*), mature- (*Col2a1*), and late-stage (*Indian hedgehog, Ihh*) chondrocytes. Consistent with the Alcian blue staining, all of the markers of chondrocytes were strongly repressed by exposure to Nifedipine, while the level of *Sox9* was significantly increased following exposure to A23187 (Fig. 3*C*).

The fact that Nifedipine blocks expression of the early cartilage marker *Sox9* suggests that the L-type VGCCs act to promote the earliest stages of chondrogenesis. To further test this, we exposed micromass cultures to Nifedipine for various time windows. When the cells were treated with the drug from day 0 through day 2 of culture (Fig. 3 *D–F*), there was a near total suppression of chondrogenic differentiation, as assessed by Alcian blue staining and *Sox9*, *Col2a1*, and *Ihh* expression. In contrast, treatment from day 1 to day 3, or from day 2 to day 4, showed a much weaker effect, with a mild decrease in Alcian blue staining and *Col2al* expression, and *Sox9* levels comparable to those in control cultures. Nifedipine treatment appeared to affect only chondrocyte differentiation rather than cell proliferation because the size of the micromass cultures was similar between the cultures (*SI Appendix*, Fig. S4). Taken together, these results strongly implicate a role for L-type VGCCs in

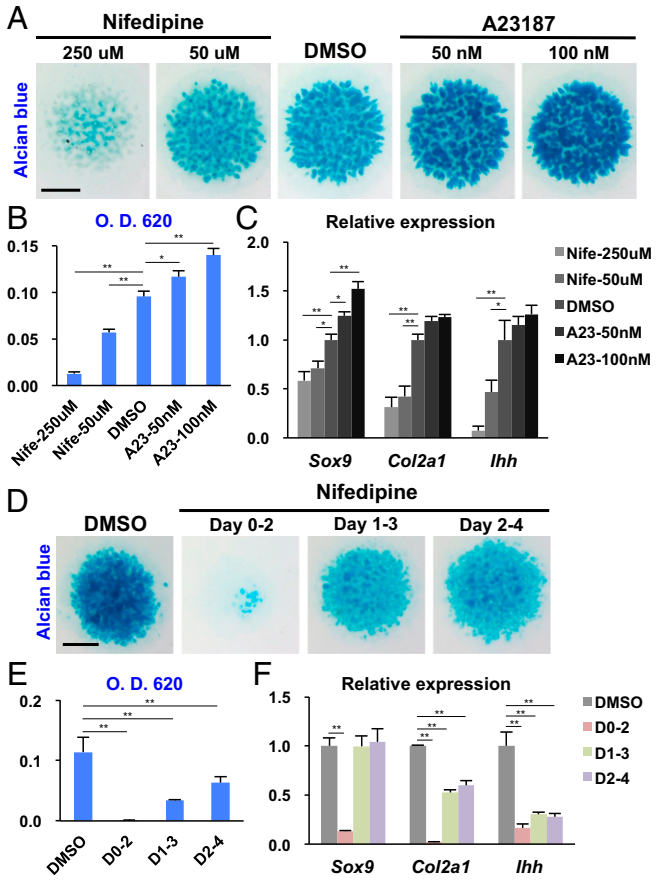

Fig. 3. Ca^{2+} influx via L-type Ca^{2+} channels regulates chondrogenesis of chicken limb bud mesenchyme in vitro. (*A*) HH20 chicken limb bud cells were micromass-cultured in the presence of Nifedipine (50 μM or 250 μM) and A23187 (50 nM or 100 nM) for 5 d, and stained with Alcian blue. (*B*) Quantification of Alcian blue intensity (n = 8 for each group). (*C*) *Sox9*, *Col2a1*, and *Ihh* mRNA expression levels were measured by qPCR and normalized to *β-actin* expression (n = 8 each). (*D* and *E*) Micromass-cultured chicken cells were treated with DMSO, Nifedipine (250 μM) from days 0 to 2, days 1 to 3, or days 2 to 4, for 5 d, and stained with Alcian blue (n = 5 each). (*F*) Relative expression levels of *Sox9*, *Col2a1*, and *Ihh* were quantified by qPCR (n = 5 each). Error bars represent SEM. $^*P < 0.05$, $^{**}P < 0.01$; 1-way ANOVA multicomparison with DMSO as control. (Scale bars: 2 mm in *A* and *D*.)

modulating Ca^{2+} levels to promote the first steps in chondrogenesis of limb mesenchyme.

$Ca_V1.2$, an L-Type Voltage-Gated Ca^{2+} Channel, Is Essential for Skeletal Development in the Mouse Limb. Based on these results, we next interrogated the role of L-type VGCCs during limb development. $Ca_V1.2$ (encoded by the *Cacnalc* gene) is known to be broadly expressed in developing mouse limbs at E11.5 (31). We confirmed broad $Ca_V1.2$ protein expression in developing mouse hindlimbs by immunohistochemistry (*SI Appendix*, Fig. S5). This expression pattern made $Ca_V1.2$ a strong candidate for mediating the L-type VGCC-dependent Ca^{2+} influx that we observed during chondrogenesis. The *Cacnalc* gene has previously been deleted in mice, but the mutants exhibit an early embryonic lethality (32), precluding an analysis of limb-stage chondrogenesis. We therefore derived limb-specific *Cacnalc* conditional mutant mice by crossing the limb-specific *Prx1*-CreER lines with mice harboring a floxed allele. Control mice carrying either the *Cacnalc*$^{fl/fl}$ allele, or the *Prx1*-CreER alone, did not show limb malformations at E18.5 following tamoxifen treatment (Fig. 4*A* and *SI Appendix*, Fig. S6). In contrast mice carrying both the *Prx1*-CreER and the *Cacna1c*$^{fl/fl}$ allele (hereafter referred to as "mutant" mice) had notable limb abnormalities (Fig. 4*B*). (Note: For this analysis we focused on transgenic mice that were homozygous for the *Prx1*-CreER allele, as they achieve a faster deletion of the floxed allele than *Prx1*-Cre heterozygotes.) As $Ca_V1.2$ proteins were depleted in the mutant mouse limbs upon tamoxifen injections (*SI Appendix*, Fig. S7), the phenotypes were likely to be attributable to defects in Ca^{2+} signaling via $Ca_V1.2$. Most prominently, *Cacnalc* mutant mice displayed shortened limbs (Fig. 4). For example, the mutant hindlimbs were 76.9% of the length of controls (Fig. 4*C*). The mutant hindlimbs were also missing digits. Forelimbs showed similar kinds of defects; however, in general, the phenotypes were relatively more severe in hindlimbs than forelimbs (Fig. 4 *C* and *D*), correlating with a relatively higher mRNA expression level of *CreER* in hindlimb buds of E10.5 embryos than in forelimbs (*SI Appendix*, Fig. S8). Mice displayed similar kinds of phenotypes, albeit to a lesser extent, when tamoxifen was administered at E10.5

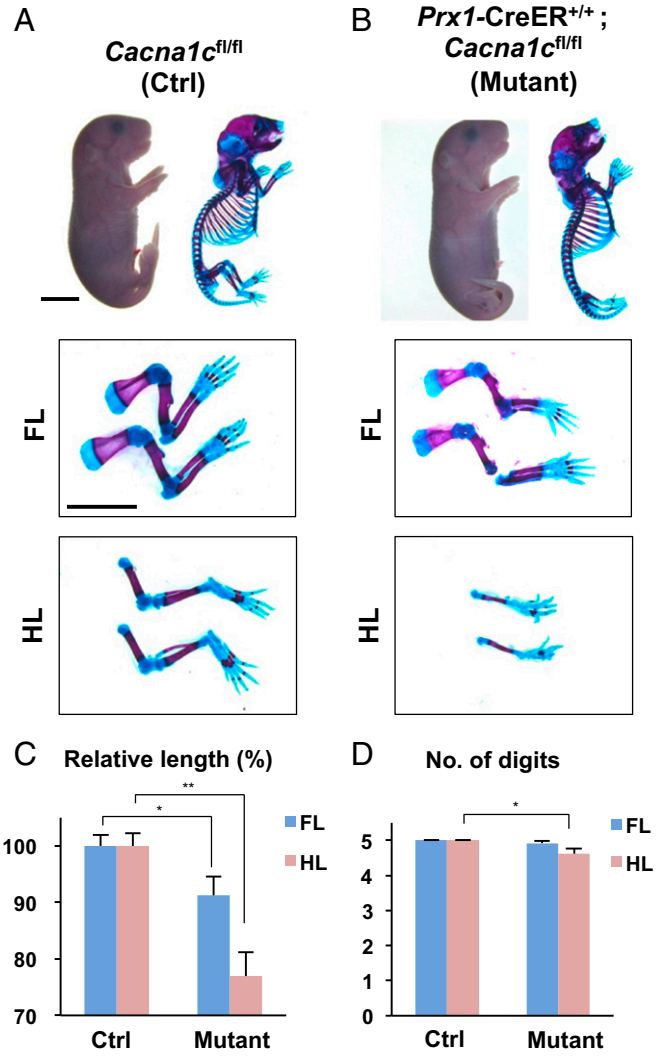

Fig. 4. $Ca_V1.2$ is required for development of skeletal elements in mouse limbs. (*A* and *B*) Alcian blue/Alizarin red skeletal preparations of E18.5 *Cacna1c*$^{fl/fl}$ (control, *A*), and *Prx1*-CreER$^{+/+}$; *Cacna1c*$^{fl/fl}$ mouse embryos (mutant, *B*). Tamoxifen injections were performed at E9.5 and E10.5. Forelimbs (FL) and hindlimbs (HL) are separately displayed. (Scale bars: 5 mm in *A*.) (*C* and *D*) Quantification for relative length of the limbs (*C*) and the number of digits (*D*) of controls (n = 20 limbs) and mutants (n = 26). Error bars represent SEM. $^*P < 0.05$, $^{**}P < 0.01$.

and E11.5 rather than at E9.5 and E10.5 (*SI Appendix*, Fig. S9). These data demonstrated a role for $Ca_V1.2$ in limb development.

Lack of $Ca_V1.2$ Activity Affects Cell Death but Not Proliferation in the Early Limb Bud. Given that the mutant limbs were shorter than the wild-type, we scrutinized whether cell proliferation and programmed cell death were affected in the differentiating limb mesenchyme of the mutants, making use of a mitotic marker, phosphorylated histone H3 (pH3), and an apoptotic marker, cleaved caspase3 (Cas3). Quantification of $pH3^+$ cells in the forelimb and hindlimb buds at E11.5 showed no significant differences between control and mutant limbs (Fig. 5 *A–D* and *I*). In contrast, Cas3 analyses revealed that excess cell death occurred in the limb buds of the mutant (Fig. 5 *E–H* and *J*). While the observed cell death might contribute to the overall decrease in the size of the mutant limbs, it is notable that the apoptotic cells are distributed across the entire limb bud and, if anything, are present to a lesser extent in the core of the limb bud where chondrogenesis takes place. Thus, decreased survival would not be a probable explanation for the observed defects in the skeletal elements.

$Ca_V1.2$ Controls Chondrocyte Differentiation by Regulating Sox9 Expression. To better understand the skeletal abnormalities in the $Ca_V1.2$-deficient limbs, we examined the pattern of chondrogenesis during cartilage differentiation by staining with the marker *Col2al* at E13.5 (Fig. 6 *A* and *B*). Not only are less chondrogenic cells observed, the spacing of the skeletal elements (for example, between the digits of the mutant limbs) was also misregulated. To see if the earliest steps of chondrocyte differentiation were disturbed in the $Ca_V1.2$-deficient mice in vivo, as seen in the Nifedipine-treated micromass cultures, we examined Sox9 expression in the mutant mice at both E11.5 and E13.5 (Fig. 6 *A–D*). Indeed, immunostaining for Sox9 protein demonstrated reduction of the proteins in the hindlimb buds of mutant embryos at both stages (Fig. 6 *A–D*). Consistent with this, qPCR analyses revealed significant decrease of *Sox9* as well as the late-stage chondrogenic marker *Aggrecan1* (*Agc1*) (Fig. 6*E*). This effect on chondrogenic differentiation appears to be specific, as no differences (examined by qPCR) were seen between control and $Ca_V1.2$ mutant limbs in the expression of other key genes known to regulate limb pattern, including genes acting through the Wnt pathway (*Axin2*), the Fgf pathway (*Fgf8*, *Fgf10*, *Dusp6*), the hedgehog pathway (*Shh*, *Ptch1*), genes involved in regulating key domains of cell death (*Msx2*), or genes establishing a proximodistal pattern (*Hoxd13, Meis2*) (*SI Appendix*, Fig. S10). The 1 exception to this was when we evaluated proximodistal markers by in situ hybridization. Proximodistal patterning in limbs was examined using *Meis1* and *Hoxa13* as proximal and distal markers, respectively (*SI Appendix*, Fig. S11). *Hoxa13* was distally localized in an apparently normal expression domain at both E11.5 and E13.5 in mutant embryos (*SI Appendix*, Fig. S11 *B* and *D*). *Meis1* was similarly detected at the correct location in the proximal third of the limb bud at E11.5. However, unlike *Hoxa13*, which continues to be expressed around the differentiating skeletal elements at E13.5, *Meis1* is normally down-regulated by E13.5 as chondrogenic differentiation proceeds. However, in the mutant limbs, *Meis1* expression is aberrantly sustained at E13.5 (*SI Appendix*, Fig. S11 *A* and *C*). Maintenance of *Meis1* expression is likely secondary to the defective differentiation seen in the mutant limbs.

These data indicate a specific role of $Ca_V1.2$ in regulating the earliest steps of chondrogenic differentiation. The Bone morphogenetic protein (Bmp) pathway is also known to play a critical role in the initiation of chondrogenesis in the developing limb (33–35). To ask whether the reduction of Sox9 is attributable to failure of Bmp activation, we performed staining of phospho-Smad (pSmad), a readout of Bmp signaling. pSmad staining was seen in the peripheral regions of E11.5 in equivalent domains in the mutant and control limb buds (Fig. 6 *F* and *G*). Similarly, at E13.5, signals were observed interdigitally in both the controls and mutants (Fig. 6 *F* and *G*). These results suggest that $Ca_V1.2$ regulates chondrogenesis in a Bmp-independent manner.

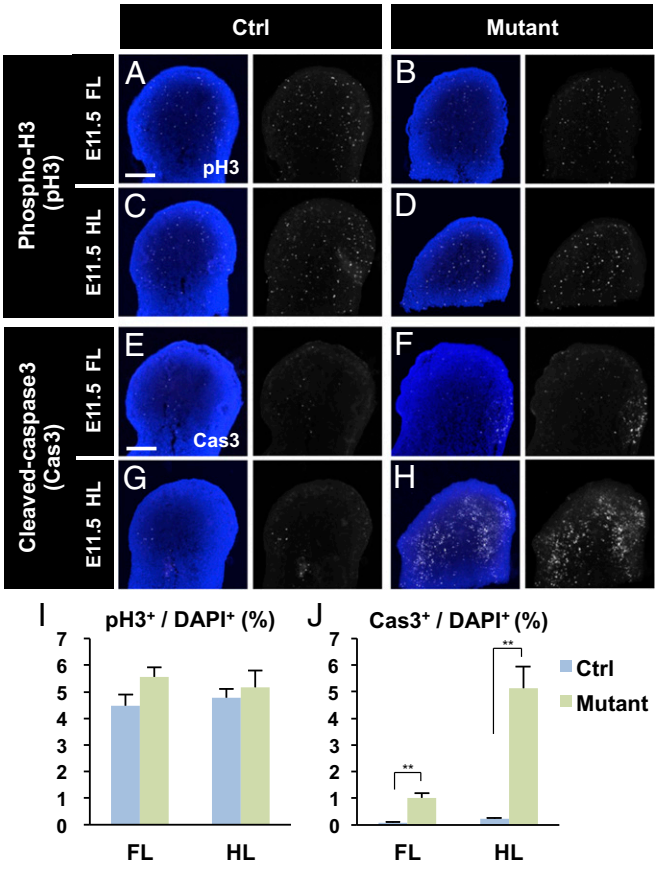

Fig. 5. Increased cell death in $Ca_V1.2$ mutant limb buds. (*A–H*) Sagittal sections of fore- or hindlimb buds from E11.5 Control (*A*, *C*, *E*, and *G*) and mutant mouse embryos (*B*, *D*, *F*, and *H*) were stained with antibodies for phospho-histone H3 (pH3; *A–D*) or cleaved-caspase3 (Cas3; *E–H*). (Scale bars: 200 μm in *A* and *E*.) (*I* and *J*) Quantification of the number of $pH3^+$ or $Cas3^+$ cells in the limb buds ($n = 12$ each for pH3-counting, $n = 18$ each for Cas3-counting). Error bars represent SEM. $^{**}P < 0.01$.

NFATc1 Mediates Ca^{2+}/$Ca_V1.2$ Signaling during Limb Mesenchyme Chondrogenesis. Since the impact of $Ca_V1.2$ on limb bud chondrogenesis appears to be independent of Bmp signaling, we considered the possibility that its effect could be cell-autonomous. One important set of intracellular effectors of Ca^{2+} signaling is the NFAT (nuclear factor of activated T-cells) family of transcription factors. There are 5 members of the NFAT family (NFATc1 to -5), and subcellular localization of NFATs, except NFATc5, is known to be regulated by Ca^{2+} signaling. In the presence of Ca^{2+}, calmodulin, a well-established calcium sensor, initiates a cascade leading to dephosphorylation of the NFAT proteins, thereby activating them and resulting in their nuclear translocation. We observed that 1 of these members, *NFATc1*, is broadly expressed in the early mouse limb bud and is very specifically expressed in chondrogenic regions, such as in the developing digits (Fig. 7*A*). To verify that NFATc1 expression coincides with mesenchymal chondrogenesis, we looked at expression of NFATc1 proteins in cultured limb mesenchyme harvested from either control or $Ca_V1.2$ mutant embryos. Nuclear localized NFATc1 (the active form of NFATc1) and Sox9 protein colocalize in the chondrogenic micromass cells in control cultures. Both proteins were seen to a lesser degree in the mutant cells

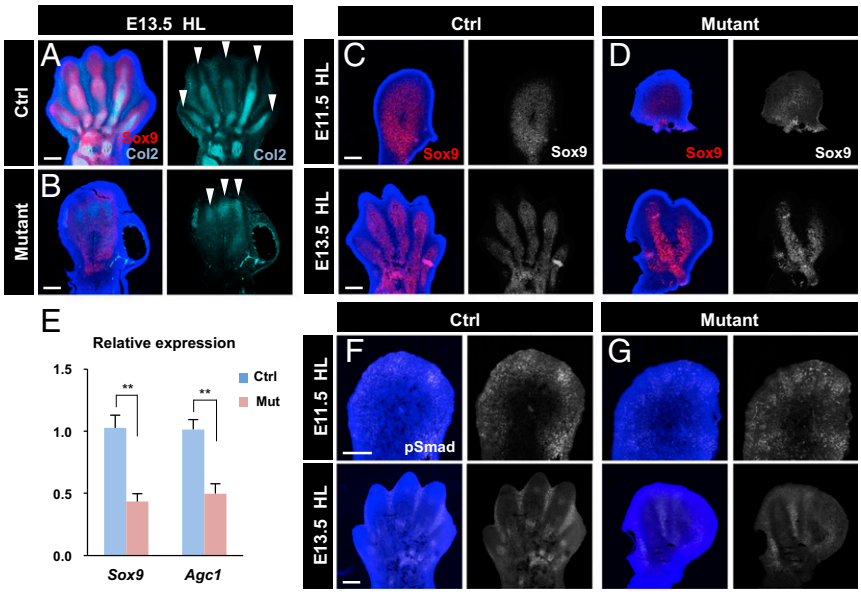

Fig. 6. Requirement of $Ca_V1.2$ for chondrocyte differentiation in mouse limbs. (*A* and *B*) Sagittal sections of E13.5 control (*A*) and mutant hindlimbs (*B*) were stained with antibodies for Sox9 (red) and Col2 (cyan). Cartilage elements were marked by anti-Col2 antibodies as indicated by arrowheads. (*C* and *D*) Sagittal views of hindlimbs of E11.5 and E13.5 mouse embryos. Chondrocytes were visualized by immunostaining against Sox9. (*E*) *Sox9* and *Agc1* expression levels were measured by qPCR and normalized to *β-actin* expression ($n = 7$ for each group). (*F* and *G*) Immunostaining of phosphorylated Smad1/5 (pSmad) in E11.5 and E13.5 hindlimbs from control (*F*) and mutant embryos (*G*). Error bars represent SEM. $^{**}P < 0.01$. (Scale bars: 200 μm in *A*–*C* and *F*.)

(Fig. 7 *B*–*D*). Moreover, the fluorescent intensity of NFATc1 and Sox9 signals were positively correlated with one another (Fig. 7*E*).

To test whether NFATc1 is capable of activating the chondrogenic program in vivo, we introduced a plasmid that bicistronically expresses $NFATc1^{nuc}$ (a constitutively activated, Ca^{2+}-independent form of the protein) (36) and ZsGreen1, along with a transposase-expressing vector, into chicken limb progenitors by electroporation (Fig. 7 *F* and *G*). The $NFATc1^{nuc}$-electroporated cells form $Sox9^+$ aggregates ectopically (Fig. 7*G*), showing that NFATc1 does indeed have prochondrogenic activity.

We reasoned if $Ca_V1.2$ regulates chondrogenesis through modulation of the cartilage-promoting activity of NFATc1, then introduction of an activated form of NFATc1 should be able to restore chondrogenesis in the context of the $Ca_V1.2$ mutant. Harvested limb mesenchyme was placed into micromass cultures and infected with a lentivirus carrying either mCherry (control) or $NFATc1^{nuc}$ (*SI Appendix*, Fig. S12). When $NFATc1^{nuc}$ was overexpressed, the reduced chondrocyte formation was partially restored, as assessed by Alcian blue intensity (Fig. 7 *H* and *I*).

Discussion

We have identified the L-type voltage-gated channel $Ca_V1.2$ as a key player in chondrogenesis, and more broadly implicated the regulation of membrane potential as a crucial parameter in controlling cell differentiation decisions during limb development. We started by interrogating the V_{mem} dynamics during limb development in both chick and mouse embryos. DiBAC staining particularly highlighted differentiating chondrocytes as being strongly depolarized. Indeed, depolarization appears to be crucial for chondrocyte differentiation as the pharmacological inhibition of ENaC, a channel known to modulate membrane depolarization in other contexts (9, 37), blocked cartilage formation in micromass cultures, and Ca^{2+} transients activated by depolarization are themselves required for cartilage formation. It is, however, unclear whether ENaC itself is required for limb cartilage formation in vivo.

In contrast to the depolarization observed in differentiating chondrocytes, undifferentiated limb mesenchyme is relatively hyperpolarized, excluding DiBAC staining, and taking up the low-voltage indicator CC2-DMPE. In zebrafish fins, gain-of-function mutations in *kcnk5b*, a gene that encodes a 2-pore domain K^+ channel, lead to membrane hyperpolarization and significantly promote cell proliferation of fin mesenchyme (8). This raises the possibility that the hyperpolarization we observe in the early chick and mouse limb-bud mesenchyme could reflect a role in modulating the proliferation within the early limb bud.

Although $Ca_V1.2$ was previously known to be expressed in limb chondrocytes, its role in promoting chondrogenesis had not been elucidated. A missense mutation of *Cacna1c* (G406R), which is constitutively activated, and hence inappropriately increases intracellular Ca^{2+} concentration, causes limb malformation in Timothy syndrome patients (23), and limb-specific overexpression of the G406R mutant in mice resulted in increase of bone mass in the limbs (38). These animals did not, however, display aberrant chondrogenesis, per se, indicating that $Ca_V1.2$ activity is not sufficient on its own to drive these processes. A requirement of VGCCs in digit formation was implied in a second study, in which Nifedipine was administered to pregnant rabbits and the fetuses showed reduction of digits and abnormal structure of phalanges (39). It was, however, concluded that these phalangeal phenotypes were secondarily induced by decreased blood flow caused by excessive hypotension, rather than direct inhibitory actions of the blocker on VGCCs (40, 41). In contrast, our analysis of limb-specific $Ca_V1.2$ cKO mice, supported by in vitro culture studies, strongly indicate that $Ca_V1.2$ plays an essential role in regulating chondrogenesis in the limb buds.

$Ca_V1.2$ is important, not only for chondrocyte differentiation, but also for protecting limb mesenchyme from inappropriate apoptosis. Bmp signaling has many roles in vertebrate limb development, including initiating chondrogenic differentiation and inducing programmed cell death to sculpt the autopod (35, 42). Even though expression levels of *Sox9* were decreased in the mutant limb buds, pSmad proteins were seen at similar levels,

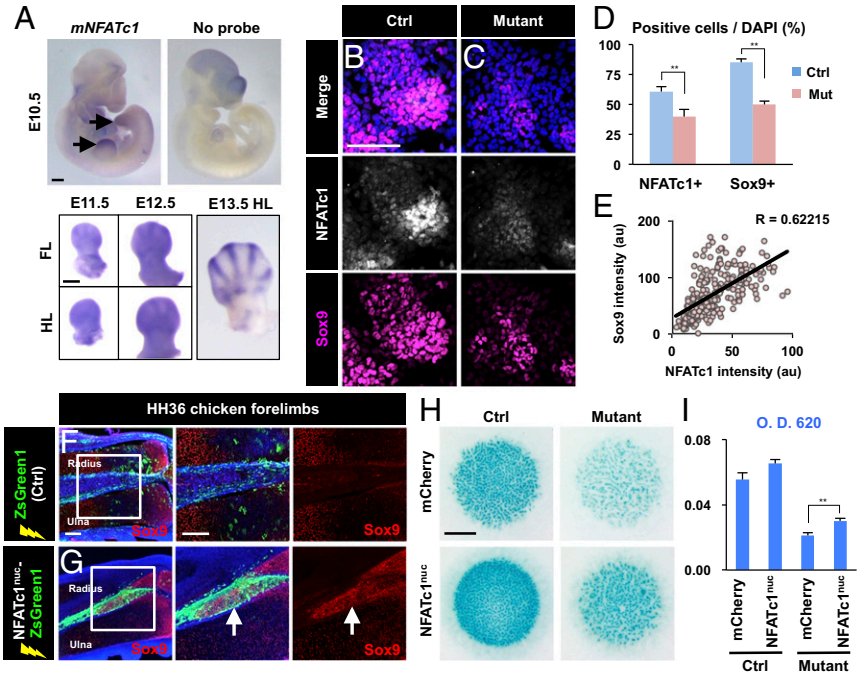

Fig. 7. NFATc1 is reduced in the $Ca_V1.2$ cKO cells and is sufficient to up-regulate chondrocyte differentiation in vivo and in vitro. (*A*) mRNA expression patterns of *NFATc1* in E10.5, E11.5, E12.5, and E13.5 mouse limbs. Arrows mark *NFATc1* expression at both fore- and hindlimb buds. (*B* and *C*) Immunostaining for NFATc1 and Sox9 in cultured mouse limb cells harvested from E11.5 control (*B*) and mutant limb buds (*C*). (*D*) Quantification of the number of $NFATc1^+$ or $Sox9^+$ cells in the cultured cells ($n = 3,436$ cells for control, $n = 1,585$ cells for mutant group). (*E*) Measurement of fluorescent intensity for NFATc1 and Sox9 signals ($n = 270$ cells from control group). (*F* and *G*) Plasmids carrying ZsGreen1 (control, *F*) or $NFATc1^{nuc}$-IRES-ZsGreen1 (*G*) were electroporated into chicken forelimbs. Misexpression of $NFATc1^{nuc}$ resulted in inducing a $Sox9^+$ ectopic aggregate (an arrow in *G*; $n = 5$ of 15), which was not seen in the controls ($n = 0$ of 15). (*H* and *I*) mCherry or $NFATc1^{nuc}$ was overexpressed in micromass-cultured cells obtained from E11.5 control and mutant embryos by using lentiviruses (see *SI Appendix*, Fig. S10 for experimental procedures). (*I*) Quantification of Alcian blue staining ($n = 8$ for each group). Error bars represent SEM. $^{**}P < 0.01$. (Scale bars: 500 μm in *A*, 100 μm in *B*, 200 μm in *F*, and 2 mm in *H*.)

compared to the controls, suggesting that Bmp signals were activated normally in the mutants. These results suggest that $Ca_V1.2$ regulates *Sox9* expression independent of Bmp activity.

It has previously been shown that increases in intracellular Ca^{2+} concentration are involved in promoting chondrocyte proliferation (38, 43). However, this would appear to be independent of $Ca_V1.2$, as cKO limbs display no significant change in number of mitotic cells.

We show that $Ca_V1.2$ signaling is important for early phases of limb chondrocyte differentiation. However, $Ca_V1.2$ is not absolutely required for the initiation of chondrogenesis, as *Sox9* is detected in mutant E11.5 hindlimb buds. Moreover, the mutant mice form skeletal elements, albeit greatly reduced in size. $Ca_V1.2$ is nonetheless essential for proper differentiation at the earliest stages of skeletogenesis. $Ca_V1.2$ does not appear to be as crucial at later stages, however, as delayed tamoxifen injection causes only modest defects in cartilage formation in mouse limbs. Similarly, late Nifedipine treatment in micromass cultures does not affect Ca^{2+} transients in the cultured cells (except for myogenic cells), and only modestly affects chondrogenesis. Other Ca^{2+} channels may be responsible for Ca^{2+} influx at later stages of chondrocyte differentiation. One candidate channel is $Ca_V3.2$ because it is also expressed in limb chondrocytes and micromass-cultured limb mesenchyme from the $Ca_V3.2^{-/-}$ mice exhibited attenuated cartilage formation (22). Another ion channel that potentially regulates late chondrogenesis is TRPM7 (transient receptor potential cation channel subfamily M member 7), because TRPM7-mediated Ca^{2+} fluctuations in growth plate chondrocytes were found to be critical for chondrocyte maturation (44).

We further found that Ca^{2+} influx via $Ca_V1.2$ appeared to activate nuclear translocalization of NFATc1, which in turn up-regulated expression of *Sox9*, a master regulator for chondrocyte differentiation in the limbs. In addition to chondrogenic differentiation, *Sox9* is known to regulate proliferation and survival of differentiating limb mesenchyme (45); thus, NFATc1 and related family members, such as NFATc2 that could act synergistically with NFATc1, may be critical for multiple aspects of limb development. Consistent with our results, Lin et al. (22) previously demonstrated that Ca^{2+} entry via $Ca_V3.2$ regulated *Sox9* expression in tracheal cartilage, which was mediated by an NFATc1 binding site within the *Sox9* promoter. Also, in the pancreas, an NFATc1/c-Jun complex up-regulates *Sox9* expression, which in turn initiates pancreatic adenocarcinoma by binding to the promoter regions of *Sox9*, albeit in a different context from chondrocytes (46). This evidence suggests that the mechanistic regulation of *Sox9* expression by NFAT may be widely conserved in biological events, such as development and cancer.

Materials and Methods

Experimental Animals. White leghorn eggs were obtained from Charles River. Chicken embryos were staged according to the Hamburger and Hamilton stages (HH) (47). Mouse colonies were maintained in the vivarium at the New Research Building of Harvard Medical School. *Cacna1c*$^{tm3hfm/J}$ mice (also known as $Ca_V1.2$-floxed) were purchased from the Jackson Laboratory (Stock no. 024714). *Prx1*-CreER-IRES-GFP (*Prx1*-CreER) mice were provided by Shunichi Murakami, Case Western Reserve University, Cleveland, OH (48). Ai9 (*Gt[ROSA]26Sor*$^{tm9[CAG-tdTomato]Hze}$) and *Col2a1*-CreER (49) mouse strains were obtained from the Jackson Laboratory (Stock no. 007909 and 006774, respectively). Ai9 mice were crossed with *Col2a1*-CreER mice to obtain *Col2a1*-tdTomato reporter embryos. All animal experiments were performed under the guidelines of the Harvard Medical School Institutional Animal Care and Use Committee.

Micromass Culture and Alcian Blue Staining. Limb buds from HH20 chicken or E11.5 mouse embryos were used to generate micromass cultures. Briefly, after the surface ectoderm was removed in 0.25% Trypsin-EDTA solution (Sigma-Aldrich), limb mesenchyme was dissociated gently by pipetting and pelleted by centrifugation. The cells were redissociated, and 2×10^5 cells per 20 μL of 10% FBS/DMEM were dropped into each well of a 24-well plate. After being attached, the cells were cultured in 10% FBS/DMEM for 5 d. Alcian blue staining was performed as previously described (50). To extract Alcian blue dye, the stained cultures was incubated with 250 μL of 6 M guanidine hydrochloride for 24 h at 37 °C, and the OD of extracted Alcian blue was measured at 620 nm. Benzamil, Nifedipine, and 4-Bromo A23187 were obtained from Sigma-Aldrich.

Imaging with DiBAC$_4$(3) and CC2-DMPE. DiBAC$_4$(3) and CC2-DMPE staining was performed as previously described with slight modifications (24). DiBAC was obtained from Thermo Fisher Scientific, and was prepared in a loading buffer (160 mM NaCl, 4.5 mM KCl, 2 mM $CaCl_2$, 1 mM $MgCl_2$, 10 mM Glucose, 10 mM Hepes, 1% FBS, pH 7.4). Primary cultured limb mesenchyme was soaked at a concentration of 0.5 μg/mL for 30 min at 37.5 °C, and slice-cultured limbs were incubated with 1 μg/mL for 1 h with gently rocking at 37.5 °C, to allow for sufficient dye permeation before imaging. Sliced limb buds were embedded with 1% low melting agarose (Invitrogen) in a 35-mm glass-bottom dish (MatTek Corporation) after the incubation for the confocal imaging (Carl Zwiss LSM710). To induce membrane depolarization, sliced chicken limb buds were soaked in the loading buffer containing 40 mM K-gluconate for 10 min prior to the embedding. CC2-DMPE (Invitrogen) was used at a concentration of 5 μM that was mixed in DiBAC solution.

Skeletal Preparation. Skeletal preparations were carried out as described previously (51). The E18.5 embryos were skinned and eviscerated, and fixed in 95% ethanol overnight and then in acetone overnight at room temperature. Subsequently, embryos were stained in Alcian blue 8GX (Sigma-Aldrich) solution for 24 h at room temperature, and incubated in 1% KOH for several hours. Then, embryos were stained with Alizarin red S (Sigma-Aldrich) overnight, and permeabilized through a graded series of 1.5% KOH, 1% KOH, 1% KOH/20% glycerol, 0.6% KOH/40% glycerol, 0.4% KOH/60% glycerol, and 80% glycerol for imaging.

Tamoxifen and 4-Hydroxy Tamoxifen (4-OHT) Treatment. Tamoxifen was dissolved in corn oil (Sigma-Aldrich), and 1 mg/d of tamoxifen was given to E9.5 to E11.5 pregnant dams by intraperitoneal injections; 5 μM of 4-OHT (Calbiochem) was used for in vitro micromass culture experiments.

In Ovo Electroporation and Expression Vectors. For the in ovo electroporation, eggs were incubated for about 54 h at 38 °C. DNA solution was prepared at 4 μg/μL, and injected into the coelomic cavity of HH14 embryos. Three electric pulses of 50 V, 2 ms, were given, followed by 7 pulses of 5 V, 10 ms, with 10-ms interval between pulses (Super Electroporator NEPA21-type II, NEPA GENE). pT2A-CAGGS-IRES2-ZsGreen1 was described previously (52, 53). For pT2A-CAGGS-NFATc1^{nuc}-IRES2-ZsGreen1, coding sequences (CDS) of NFATc1^{nuc} were amplified from pCR4-huNFATc1^{nuc} (Addgene plasmid # 23988) (36) by PCR using Q5 DNA polymerase (New England Biolabs), and subcloned into pT2A-CAGGS-IRES2-ZsGreen1 by Gibson Assembly Cloning Kit (New England Biolabs). The plasmid was sequence verified prior to the electroporation. pCAGGS-T2TP was shared by Yoshiko Takahashi, Kyoto University, Kyoto, Japan. For preparation of GCaMP-labeled cells, RCAS-GCaMP6s-2A-mCherry plasmid (30) was electroporated into HH14 embryos.

Time-Lapse Imaging. For in vitro time-lapse imaging, GCaMP6s-2A-mCherry–electroporated limb mesenchymal cells were micromass-cultured on a 35-mm glass-bottom dish. The cells were cultured in 10% FBS/DMEM in an incubation chamber attached to the LSM10 confocal microscope, and images were taken every minute. For artificial depolarization, 40 mM potassium-gluconate was used, and 250 μM of Nifedipine was added to medium to inhibit Ca^{2+} transients.

Immunostaining. For immunological staining on histological sections, the following antibodies were used as described previously (54): Mouse anti-Collagen 2A1 (1:100; DSHB, II-6B3), rabbit anti-pH3 (1:1,000; Millipore, 06-570), rabbit anticleaved caspase-3 (1:300; Cell Signaling, #9661), rabbit anti-Ca_v1.2 (1:200; Alomone Laboratories, ACC-003), rabbit anti-Sox9 (1:500; Millipore, AB5535), rabbit anti-pSmad1/5 (1:300, Cell Signaling, #9516), and mouse anti-NFATc1 (1:25; Santa Cruz, sc-7294). For staining of Col2A1 and Ca_V1.2, an antigen retrieval using Target Retrieval Solution (DAKO, S2369) was performed in advance of blocking. To detect pSmad, TSA Plus Cy3 system (PerkinElmer) was used as previously described (54).

qPCR. RNA was extracted using the RNeasy Mini Kit (Qiagen) and reverse-transcribed by SuperScript III First-Strand Synthesis System (Thermo Fisher). PCR was performed by using Brilliant III Ultra-Fast SYBR Green QPCR kit (Agilent) and CFX Touch Real-Time PCR Detection System (Bio-Rad). Relative expression levels were calculated by the ΔΔCq method. Genotypes for Prx1-Cre^{ER}-GFP allele was determined according to the Cq values obtained by qPCR using the SYBR Green QPCR kit. Sequences (5′-3′) of primers for qPCR are as follows:

cßactin-F, TCTGACTGACCGCGTTACTC;

cßactin-R, CCATCACACCCTGATGTCTG;

cSox9-F, AGGAAGCTGGCTGACCAGTA;

cSox9-R, CGTTCTTCACCGACTTCCTC (55);

cCol2a1-F, GGACAGCGTGGTGAGAGAGGCTT;

cCol2a1-R, TCCCTGCCTGGGAGACCGTCA (56);

cIhh-F, CATCCACTGCTCCGTCAAGT;

cIhh-R, ATGACGTGGAAGGCAGTGAG;

mßactin-F, GCTGTATTCCCCTCCATCGTG;

mßactin-R, CACGGTTGGCCTTAGGGTTCAG;

mSox9-F, TAAGTTCCCCGTGTGCATCC;

mSox9-R, TTGCCCAGAGTCTTGCTGAG;

mAgc1-F, GGTCACTGTTACCGCCACTT;

mAgc1-R, CCCCTTCGATAGTCCTGTCA;

mDusp6-F, CGGAAATGGCGATCTGCAAG;

mDusp6-R, GACGACTCGTACAGCTCCTG;

mMsx2-F, CAAGTGAAGGGGGAGGTGTA;

mMsx2-R, CAGGGACCTGACATGGAGTT;

mAxin2-F, GAGGAGATCGAGGCAGAAGC;

mAxin2-R, CACCTCTGCTGCCACAAAAC;

mFgf8-F, AGAGAGACAGTGTCCTGCCT;

mFgf8-R, TCTTCTGCCATGGCGTTGAT;

mFgf10-F, AGCGGGACCAAGAATGAAGACTGT;

mFgf10-R, CCTGCCATTGTGCTGCCAGTTAAA (57);

mMeis2-F, GTTCCGTCATTTCGTTCTCC;

mMeis2-R, CTTTCTCGCTCGCTCTCACT;

mShh-F, CCGAACGATTTAAGGAACTCACCC;

mShh-R, TGGTTCATCACAGAGATGGCCAAG (58);

mPtch1-F, GACCGGCCTTGCCTCAACCC;

mPtch1-R, CAGGGCGTGAGCGCTGACAA;

mHoxd13-F, TGTCCACTTTTGGATCCGGG;

mHoxd13-R, TTCTTCCTTCCCCGTCGGTA;

Cre-F, GCATTACCGGTCGATGCAAC;

Cre-R, ACATCTTCAGGTTCTGCGGG.

Probes and In Situ Hybridization. Mouse cDNA fragments for *NFATc1* and *Meis1* were isolated by PCR using primers (5′–3′):

NFATc1-F, ATAACGCGTGCTACAGCTGTTCATTGGGA;

NFATc1-R, ATAGCTAGCCTTGCACAGGTCCCGGTCAG;

Meis1-F, ATAACGCGTATGGCGCAAAGGTACGACGA;

Meis1-R, ATAGCTAGCGATCCTCCTTCTCTATCATC.

The PCR fragments were digested by MluI and NheI (New England Biolabs), and subcloned into pBS-D. Plasmids for generating antisense probes for

mHoxa13 were provided by Richard Maas, Brigham and Women's Hospital, Boston, MA. Whole-mount in situ hybridizations were performed as described in ref. 54. The color reaction was carried out with BM Purple (Sigma-Aldrich).

Lentivirus Production and Infection. FUW-M2rtTA (59), psPAX2, pMD2.G, and pLV-tetO-mCherry (60) plasmids were obtained from Addgene (#20342, #12260, #12259, and #70273). For FUW-tetO-NFATc1^{nuc}, PCR products of NFATc1^{nuc} CDS were introduced into FUW-tetO-MCS (Addgene plasmid #84008) (61) by using a Gibson Assembly Kit (New England Biolabs). VSV-G-coated lentiviral production was performed in 293T cells through cotransfection of lentiviral vectors with psPAX2 and pMD2.G by Polyethylenimine. Virus containing supernatant was collected 48 h after transfection, filtered through 0.45-μm SFCA syringe filters (Corning), and frozen for further use. Infection was performed on 24-well dishes for 24 h in the presence of 8 μg/mL polybrene (Sigma-Aldrich). Next, 2 μg/mL of doxycycline (Sigma-Aldrich) was used to activate M2rtTA.

Statistical Analysis. *P* values were obtained using a 2-tailed, unpaired Student's *t* test or 1-way ANOVA (GraphPad Prism 7, GraphPad Software).

Data Availability. All data generated or analyzed during this study are in the main text and *SI Appendix*, or available from the corresponding author upon request.

ACKNOWLEDGMENTS. We thank Drs. Dany S. Adams, Patrick McMillen, Juanita Mathews, and Joshua Finkelstein (Tufts University) for useful technical comments; members of the C.J.T. and Constance Cepko laboratories, especially Drs. Tyler Huycke, Changhee Lee, John J. Young, and Rose G. Long for helpful discussions. The RCAS-GCaMP6s-2A-mCherry plasmid was a kind gift from Dr. Ang Li (University of Southern California). This work was supported by the Allen Discovery Center program through The Paul G. Allen Frontiers Group (to M.L. and C.J.T.), and NIH Grant HD03443 (to C.J.T.). Y.A. is a recipient of fellowships of the Naito Foundation and Japan Society for the Promotion of Science (JSPS).

1. M. Levin, G. Pezzulo, J. M. Finkelstein, Endogenous bioelectric signaling networks: Exploiting voltage gradients for control of growth and form. *Annu. Rev. Biomed. Eng.* **19**, 353–387 (2017).
2. E. Bates, Ion channels in development and cancer. *Annu. Rev. Cell Dev. Biol.* **31**, 231–247 (2015).
3. D. S. Adams, A. Masi, M. Levin, H^+ pump-dependent changes in membrane voltage are an early mechanism necessary and sufficient to induce Xenopus tail regeneration. *Development* **134**, 1323–1335 (2007).
4. M. T. Belus *et al*., Kir2.1 is important for efficient BMP signaling in mammalian face development. *Dev. Biol.* **444** (suppl. 1), S297–S307 (2018).
5. E. K. Breuer *et al*., Potassium channel activity controls breast cancer metastasis by affecting β-catenin signaling. *Cell Death Dis.* **10**, 180 (2019).
6. M. Levin, T. Thorlin, K. R. Robinson, T. Nogi, M. Mercola, Asymmetries in H+/K+-ATPase and cell membrane potentials comprise a very early step in left-right patterning. *Cell* **111**, 77–89 (2002).
7. V. P. Pai, S. Aw, T. Shomrat, J. M. Lemire, M. Levin, Transmembrane voltage potential controls embryonic eye patterning in Xenopus laevis. *Development* **139**, 313–323 (2012).
8. S. Perathoner *et al*., Bioelectric signaling regulates size in zebrafish fins. *PLoS Genet.* **10**, e1004080 (2014).
9. D. Petrik *et al*., Epithelial sodium channel regulates adult neural stem cell proliferation in a flow-dependent manner. *Cell Stem Cell* **22**, 865–878.e8 (2018).
10. A. S. Tseng, W. S. Beane, J. M. Lemire, A. Masi, M. Levin, Induction of vertebrate regeneration by a transient sodium current. *J. Neurosci.* **30**, 13192–13200 (2010).
11. A. Tseng, M. Levin, Cracking the bioelectric code: Probing endogenous ionic controls of pattern formation. *Commun. Integr. Biol.* **6**, e22595 (2013).
12. M. Levin, Endogenous bioelectrical networks store non-genetic patterning information during development and regeneration. *J. Physiol.* **592**, 2295–2305 (2014).
13. K. Deisseroth *et al*., Excitation-neurogenesis coupling in adult neural stem/progenitor cells. *Neuron* **42**, 535–552 (2004).
14. W. A. Catterall, Voltage-gated calcium channels. *Cold Spring Harb. Perspect. Biol.* **3**, a003947 (2011).
15. P. Bijlenga *et al*., T-type alpha 1H Ca2+ channels are involved in Ca2+ signaling during terminal differentiation (fusion) of human myoblasts. *Proc. Natl. Acad. Sci. U.S.A.* **97**, 7627–7632 (2000).
16. B. R. Wamhoff *et al*., L-type voltage-gated Ca^{2+} channels modulate expression of smooth muscle differentiation marker genes via a rho kinase/myocardin/SRF-dependent mechanism. *Circ. Res.* **95**, 406–414 (2004).
17. S. S. Rosenberg, N. C. Spitzer, Calcium signaling in neuronal development. *Cold Spring Harb. Perspect. Biol.* **3**, a004259 (2011).
18. A. B. Toth, A. K. Shum, M. Prakriya, Regulation of neurogenesis by calcium signaling. *Cell Calcium* **59**, 124–134 (2016).
19. L. Kaestner, X. Wang, L. Hertz, I. Bernhardt, Voltage-activated ion channels in non-excitable cells–A viewpoint regarding their physiological justification. *Front. Physiol.* **9**, 450 (2018).
20. C. Pinet, S. Antoine, A. G. Filoteo, J. T. Penniston, A. Coulombe, Reincorporated plasma membrane Ca^{2+}-ATPase can mediate B-Type Ca^{2+} channels observed in native membrane of human red blood cells. *J. Membr. Biol.* **187**, 185–201 (2002).
21. Y. Shao, M. Alicknavitch, M. C. Farach-Carson, Expression of voltage sensitive calcium channel (VSCC) L-type Cav1.2 (alpha1C) and T-type Cav3.2 (alpha1H) subunits during mouse bone development. *Dev. Dyn.* **234**, 54–62 (2005).
22. S. S. Lin *et al*., Cav3.2 T-type calcium channel is required for the NFAT-dependent Sox9 expression in tracheal cartilage. *Proc. Natl. Acad. Sci. U.S.A.* **111**, E1990–E1998 (2014).
23. I. Splawski *et al*., Ca(V)1.2 calcium channel dysfunction causes a multisystem disorder including arrhythmia and autism. *Cell* **119**, 19–31 (2004).
24. D. S. Adams, M. Levin, Measuring resting membrane potential using the fluorescent voltage reporters $DiBAC_4(3)$ and CC2-DMPE. *Cold Spring Harb. Protoc.* **2012**, 459–464 (2012).
25. J. Y. Lan, C. Williams, M. Levin, L. D. Black, 3rd, Depolarization of cellular resting membrane potential promotes neonatal cardiomyocyte proliferation in vitro. *Cell. Mol. Bioeng.* **7**, 432–445 (2014).
26. A. I. Caplan, Effects of the nicotinamide-sensitive teratogen3-acetylpyridine on chick limb cells in culture. *Exp. Cell Res.* **62**, 341–355 (1970).
27. M. Shakibaei, A. Mobasheri, Beta1-integrins co-localize with Na, K-ATPase, epithelial sodium channels (ENaC) and voltage activated calcium channels (VACC) in mechanoreceptor complexes of mouse limb-bud chondrocytes. *Histol. Histopathol.* **18**, 343–351 (2003).
28. Z. Varga *et al*., Switch of voltage-gated K+ channel expression in the plasma membrane of chondrogenic cells affects cytosolic Ca^{2+}-oscillations and cartilage formation. *PLoS One* **6**, e27957 (2011).
29. T. W. Chen *et al*., Ultrasensitive fluorescent proteins for imaging neuronal activity. *Nature* **499**, 295–300 (2013).
30. A. Li *et al*., Calcium oscillations coordinate feather mesenchymal cell movement by SHH dependent modulation of gap junction networks. *Nat. Commun.* **9**, 5377 (2018).
31. K. V. Ramachandran *et al*., Calcium influx through L-type CaV1.2 Ca^{2+} channels regulates mandibular development. *J. Clin. Invest.* **123**, 1638–1646 (2013).
32. C. Seisenberger *et al*., Functional embryonic cardiomyocytes after disruption of the L-type alpha1C (Cav1.2) calcium channel gene in the mouse. *J. Biol. Chem.* **275**, 39193–39199 (2000).
33. C. Healy, D. Uwanogho, P. T. Sharpe, Regulation and role of Sox9 in cartilage formation. *Dev. Dyn.* **215**, 69–78 (1999).
34. H. Shimizu, S. Yokoyama, H. Asahara, Growth and differentiation of the developing limb bud from the perspective of chondrogenesis. *Dev. Growth Differ.* **49**, 449–454 (2007).
35. H. Zou, L. Niswander, Requirement for BMP signaling in interdigital apoptosis and scale formation. *Science* **272**, 738–741 (1996).
36. M. M. Winslow *et al*., Calcineurin/NFAT signaling in osteoblasts regulates bone mass. *Dev. Cell* **10**, 771–782 (2006).
37. S. Chifflet, J. A. Hernández, S. Grasso, A possible role for membrane depolarization in epithelial wound healing. *Am. J. Physiol. Cell Physiol.* **288**, C1420–C1430 (2005).
38. C. Cao *et al*., Increased Ca^{2+} signaling through $Ca_V1.2$ promotes bone formation and prevents estrogen deficiency-induced bone loss. *JCI Insight* **2**, e95512 (2017).
39. B. R. Danielsson, S. Reiland, E. Rundqvist, M. Danielson, Digital defects induced by vasodilating agents: Relationship to reduction in uteroplacental blood flow. *Teratology* **40**, 351–358 (1989).
40. B. R. Danielsson *et al*., Histological and in vitro studies supporting decreased uteroplacental blood flow as explanation for digital defects after administration of vasodilators. *Teratology* **41**, 185–193 (1990).
41. C. Matta, R. Zákány, A. Mobasheri, Voltage-dependent calcium channels in chondrocytes: Roles in health and disease. *Curr. Rheumatol. Rep.* **17**, 43 (2015).
42. T. Lindsten *et al*., The combined functions of proapoptotic Bcl-2 family members bak and bax are essential for normal development of multiple tissues. *Mol. Cell* **6**, 1389–1399 (2000).
43. Q. Q. Wu, Q. Chen, Mechanoregulation of chondrocyte proliferation, maturation, and hypertrophy: Ion-channel dependent transduction of matrix deformation signals. *Exp. Cell Res.* **256**, 383–391 (2000).
44. N. Qian *et al*., TRPM7 channels mediate spontaneous Ca^{2+} fluctuations in growth plate chondrocytes that promote bone development. *Sci. Signal.* **12**, eaaw4847 (2019).
45. H. Akiyama, M. C. Chaboissier, J. F. Martin, A. Schedl, B. de Crombrugghe, The transcription factor Sox9 has essential roles in successive steps of the chondrocyte differentiation pathway and is required for expression of Sox5 and Sox6. *Genes Dev.* **16**, 2813–2828 (2002).
46. N. M. Chen *et al*., NFATc1 links EGFR signaling to induction of Sox9 transcription and acinar-ductal transdifferentiation in the pancreas. *Gastroenterology* **148**, 1024–1034.e9 (2015).
47. V. Hamburger, H. L. Hamilton, A series of normal stages in the development of the chick embryo. 1951. *Dev. Dyn.* **195**, 231–272 (1992).
48. A. Kawanami, T. Matsushita, Y. Y. Chan, S. Murakami, Mice expressing GFP and CreER in osteochondro progenitor cells in the periosteum. *Biochem. Biophys. Res. Commun.* **386**, 477–482 (2009).
49. E. Nakamura, M. T. Nguyen, S. Mackem, Kinetics of tamoxifen-regulated Cre activity in mice using a cartilage-specific CreER(T) to assay temporal activity windows along the proximodistal limb skeleton. *Dev. Dyn.* **235**, 2603–2612 (2006).
50. H. S. Seo, R. Serra, Deletion of Tgfbr2 in Prx1-cre expressing mesenchyme results in defects in development of the long bones and joints. *Dev. Biol.* **310**, 304–316 (2007).

51. K. L. Cooper *et al*., Patterning and post-patterning modes of evolutionary digit loss in mammals. *Nature* **511**, 41–45 (2014).
52. Y. Atsuta, Y. Takahashi, Early formation of the Müllerian duct is regulated by sequential actions of BMP/Pax2 and FGF/Lim1 signaling. *Development* **143**, 3549–3559 (2016).
53. A. Urasaki, G. Morvan, K. Kawakami, Functional dissection of the Tol2 transposable element identified the minimal cis-sequence and a highly repetitive sequence in the subterminal region essential for transposition. *Genetics* **174**, 639–649 (2006).
54. Y. Atsuta, Y. Takahashi, FGF8 coordinates tissue elongation and cell epithelialization during early kidney tubulogenesis. *Development* **142**, 2329–2337 (2015).
55. K. L. Cooper *et al*., Initiation of proximal-distal patterning in the vertebrate limb by signals and growth. *Science* **332**, 1083–1086 (2011).
56. Y. J. Guan, X. Yang, L. Wei, Q. Chen, MiR-365: A mechanosensitive microRNA stimulates chondrocyte differentiation through targeting histone deacetylase 4. *FASEB J.* **25**, 4457–4466 (2011).
57. I. Williamson *et al*., Anterior-posterior differences in HoxD chromatin topology in limb development. *Development* **139**, 3157–3167 (2012).
58. R. Zhang *et al*., SHH protein variance in the limb bud is constrained by feedback regulation and correlates with altered digit patterning. *G3 (Bethesda)* **7**, 851–858 (2017).
59. D. Hockemeyer *et al*., A drug-inducible system for direct reprogramming of human somatic cells to pluripotency. *Cell Stem Cell* **3**, 346–353 (2008).
60. C. Kubaczka *et al*., Direct induction of trophoblast stem cells from murine fibroblasts. *Cell Stem Cell* **17**, 557–568 (2015).
61. T. Panciera *et al*., Induction of expandable tissue-specific stem/progenitor cells through transient expression of YAP/TAZ. *Cell Stem Cell* **19**, 725–737 (2016).